



Review

# Review of the Hydrogen Permeability of the Liner Material of Type IV On-Board Hydrogen Storage Tank

Ying Su <sup>1,2</sup>, Hong Lv <sup>1,2,\*</sup>, Wei Zhou <sup>1,2</sup> and Cunman Zhang <sup>1,2</sup>

<sup>1</sup> School of Automotive Studies, Tongji University, Shanghai 201804, China; shmily\_suying@163.com (Y.S.); wzhou@tongji.edu.cn (W.Z.); zhangcunman@tongji.edu.cn (C.Z.)

<sup>2</sup> Clean Energy Automotive Engineering Center, Tongji University, Shanghai 201804, China

\* Correspondence: lvhong@tongji.edu.cn

**Abstract:** The hydrogen storage tank is a key parameter of the hydrogen storage system in hydrogen fuel cell vehicles (HFCVs), as its safety determines the commercialization of HFCVs. Compared with other types, the type IV hydrogen storage tank which consists of a polymer liner has the advantages of low cost, lightweight, and low storage energy consumption, but meanwhile, higher hydrogen permeability. A detailed review of the existing research on hydrogen permeability of the liner material of type IV hydrogen storage tanks can improve the understanding of the hydrogen permeation mechanism and provide references for following-up researchers and research on the safety of HFCVs. The process of hydrogen permeation and test methods are firstly discussed in detail. This paper then analyzes the factors that affect the process of hydrogen permeation and the barrier mechanism of the liner material and summarizes the prediction models of gas permeation. In addition to the above analysis and comments, future research on the permeability of the liner material of the type IV hydrogen storage tank is prospected.



**Citation:** Su, Y.; Lv, H.; Zhou, W.; Zhang, C. Review of the Hydrogen Permeability of the Liner Material of Type IV On-Board Hydrogen Storage Tank. *World Electr. Veh. J.* **2021**, *12*, 130. <https://doi.org/10.3390/wevj12030130>

Academic Editor: Michael Fowler

Received: 14 July 2021

Accepted: 20 August 2021

Published: 22 August 2021

**Publisher's Note:** MDPI stays neutral with regard to jurisdictional claims in published maps and institutional affiliations.



**Copyright:** © 2021 by the authors. Licensee MDPI, Basel, Switzerland. This article is an open access article distributed under the terms and conditions of the Creative Commons Attribution (CC BY) license (<https://creativecommons.org/licenses/by/4.0/>).

**Keywords:** hydrogen fuel cell vehicles (HFCVs); type IV hydrogen storage tank; liner material; polymer; hydrogen permeation; prediction model

## 1. Introduction

With the increasing demand for fossil fuels internationally and domestically, the emission of carbon dioxide is increasing. Many global problems, such as climate change and global warming, come one after another [1,2]. Therefore, countries around the world have made global agreements to reduce the emission of greenhouse gases. For example, China committed to peak carbon dioxide emissions before 2030 and achieve carbon neutrality before 2060. Hydrogen is an efficient and clean energy carrier (its specific energy is about 140 MJ/kg, which is approximately 3 times that of gasoline [3].) and has the potential to substitute partly existing fuels [4]. Moreover, hydrogen has a wide source and can be produced from steam reformation of fossil fuel, biomass gasification, partial oxidation of hydrocarbons, coal gasification, and biomass fermentation [5]. For the automobile industry, to respond positively to this initiative, traditional vehicles are gradually transforming into new energy vehicles. Nowadays, HFCVs, for their high energy conversion efficiency, environmental protection, and low noise, have become one of the important directions for future automobiles development, which benefits from the special properties of hydrogen. However, there are existing challenges and barriers in the on-board hydrogen storage.

At present, on-board hydrogen storage methods can be categorized into three types: high-pressure gaseous hydrogen storage, liquid hydrogen storage, and solid-state hydrogen storage, and the most mature technology is high-pressure gaseous hydrogen storage [6]. The hydrogen storage tanks used for high-pressure gaseous hydrogen storage can be roughly divided into four types: Type I: metallic pressure vessel, Type II: metallic liner hoop wrapped with CFRP, Type III: metallic liner fully wrapped with CFRP, and Type IV: polymer liner fully wrapped with CFRP, as shown in Figure 1. The latest, the type V

hydrogen storage tank, which has 20% less weight than type IV, is made of composites without a liner. Unfortunately, it only can be used in low-pressure ranges and still needs a breakthrough [7]. The type IV hydrogen storage tank which consists of a polymer liner can greatly reduce the weight of the gas cylinder. However, its design concept is quite different from that of the hydrogen storage tank with a metal liner. To date, many companies and enterprises such as Hexagon (Norway), Faurecia (France), Quantum (USA), Toyota (Japan), etc., have successfully developed and realized the commercialization of type IV hydrogen storage tanks. For example, the series of high-pressure hydrogen storage tanks developed by Quantum named “Trishield” uses polyethylene as the liner material. Its nominal working pressure is 35 MPa and 70 MPa and the maximum capacity of the tank is 129 L, which can store 5 kg of hydrogen. The gravimetric density of the 70 MPa type IV hydrogen storage tank mounted on Toyota “Mirai II” is 6.0 wt% (The DOE stipulates that the value to be achieved by 2025 is 5.5 wt%), and its hydrogen storage capacity reaches 142.2 L, which can store 5.6 kg of hydrogen.

	V1	V2	V3	V4
composition	 All Metal	 Metal Liner + GFRP layer (hoop lap)	 Metal Liner + CFRP layer (full lap)	 Plastic Liner + CFRP layer (full lap)

**Figure 1.** Four types of hydrogen storage tanks, reproduced with permission from [8].

To ensure the safety of hydrogen storage, the metal liner material of the hydrogen storage tank is generally aluminum 6061 or 7060, steel (inox or Chrome Molybdene) [9], but the selection of polymer liner material is still being explored. Due to the good performance in the field of natural gas, high-density polyethylene (HDPE) is used as the first choice for the liner material of type IV hydrogen storage tanks. In addition, polyamide polymers are gradually being accepted because of their good gas barrier properties [10,11]. For example, the liner material of Toyota Mirai’s hydrogen storage tank is PA6 [12]. Unlike metal liner materials, polymer materials will not meet the problem named “hydrogen embrittlement”. However, the high hydrogen permeability and low mechanical strength of the polymer may be more dangerous to some extent. To ensure the safety of HFCVs, the international standard GTR 13 stipulates that the hydrogen permeation rate of the compressed hydrogen storage system should be less than  $46 \text{ Ncm}^3\text{h}^{-1}\text{L}^{-1}$  under the conditions of 1.15 times the nominal working pressure (NWP) and 55 °C. Meanwhile, at NWP and ambient temperature, ISO 19881 requires that the steady-state permeability of type IV hydrogen storage tanks in the system should be less than  $6 \text{ Ncm}^3\text{h}^{-1}\text{L}^{-1}$ .

This paper aims to survey the existing literature on the hydrogen permeability of the liner materials of the type IV hydrogen storage tanks to obtain a more thorough understanding of the hydrogen permeation characteristics and mechanisms in polymers, and then provide a solid theoretical basis for the design, development, and optimization of type IV hydrogen storage tanks. In particular, the transport process of hydrogen in polymers and the different test methods of various coefficients involved in the process are presented in Section 2. In Section 3, the paper surveys the factors affecting the process of hydrogen permeation and the barrier mechanism of liner materials. Section 4 of this paper presents the prediction models that may be used for hydrogen permeation. The paper is then concluded in Section 5.

## 2. Hydrogen Permeation in Polymers

### 2.1. Transport Process of Gas in Polymer

When assuming that the polymer film is a homogeneous, non-porous film at a given temperature, the transport of a gas molecule in the polymer can be described by a solution-diffusion model. Under normal circumstances, the entire process can be divided into the following five steps [13], as shown in Figure 2:

1. The gas passes through the limit layer on the upstream side (the high-pressure side) by diffusion.
2. The gas is absorbed by the polymer through chemical affinity or solubility.
3. The gas diffuses inside the polymer.
4. The gas is desorbed on the downstream side (the low-pressure side).
5. The gas passes through the limit layer on the downstream side by diffusion.

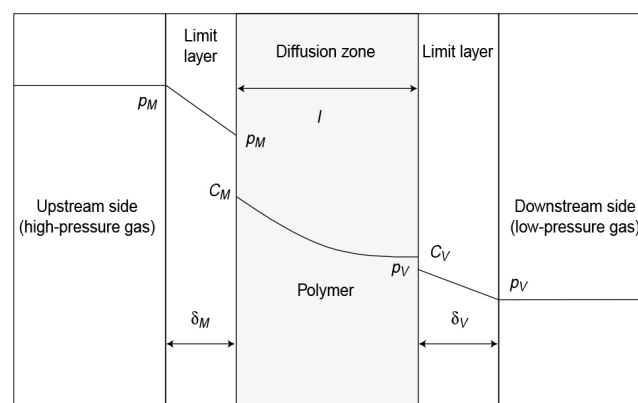


**Figure 2.** The diffusion process of gas in the polymer, reproduced with permission from [13].

Since the formation of the limit layer is difficult to observe and the resistance in the limit layer associated to the step 1 and 5 is really small, these two processes are usually negligible. According to Fick's law, the entire transport process can be divided into two parts, namely dissolution and diffusion. Dissolution is a thermodynamic term, which depends on the interaction between the penetrant and the polymer and the compressibility of the gas. The ease of dissolution is represented by the solubility coefficient  $S$ . Similarly, diffusion is a kinetic term that reflects the mobility of the penetrant in the polymer caused by random movement, expressed by the diffusion coefficient  $D$ . The gas permeability coefficient  $P$ , by definition, is used to describe the strength of the gas permeability of a polymer and it is expressed as  $P = D \times S$ . In addition, its standard unit is  $\text{mol} \cdot \text{m} \cdot \text{m}^{-2} \cdot \text{s}^{-1} \cdot \text{pa}^{-1}$ , which means we can calculate it by dividing the product of the molar mass of the permeating gas and the thickness of the sample by the sample area, the pressure difference between the two sides of the sample, and the time to reach the permeation equilibrium.

### 2.2. Test Methods of Hydrogen Permeation

To accurately describe the characteristics of the gas transmission in the polymer, it is necessary to measure the various coefficients. Fujiwara et al. reported two methods for measuring these coefficients under high pressure, which are the thermal desorption analysis (TDA) method [14] and the high-pressure hydrogen gas permeation test (HHPH) method [12,15]. In comparison, these two methods have their own merits.

#### 2.2.1. Thermal Desorption Analysis (TDA) Method

The TDA method is relatively simple. It observes the elimination of hydrogen in the sample in an unsteady state, and then infers the amount of gas permeation, and then obtains the coefficients through function fitting. The whole procedure is roughly as follows: (a) Expose the disc-shaped sample to the hydrogen environment under high pressure. (b) After a while, perform a decompression operation, and quickly put the sample after

decompression into an electric furnace at 30 °C. Then use inert gas (such as argon) to purge the desorbed hydrogen into a gas chromatograph with a molecular sieve column every 5 min. After 24 h, rapidly increase the temperature (100 °C/h) to 175 °C to eliminate residual hydrogen. (c) Integrate the measured hydrogen data to obtain the curve of the residual hydrogen content in the entire sample with time. (d) Fit the curve by Equation (1), and the hydrogen permeation amount and diffusion coefficient can be obtained. It is worth noting that when curve fitting is performed, the first measurement data mainly affected by environmental factors are usually ignored.

$$C_H(t) = \frac{32}{\pi^2} \times C_H(0) \times \left[ \sum_{n=0}^{\infty} \frac{\exp\left[-(2n+1)^2 \pi^2 D t / l^2\right]}{(2n+1)^2} \right] \left[ \sum_{n=1}^{\infty} \frac{\exp\left[D \beta_n^2 t / \rho^2\right]}{\beta_n^2} \right] \quad (1)$$

where  $C_H(t)$  is the residual hydrogen content (wt·ppm),  $D$  is the diffusion coefficient ( $\text{mm}^2/\text{s}$ ),  $l$  is the thickness of the sample,  $\rho$  is the radius of the disc-shaped sample, and  $\beta_n$  is the root of the zero-order Bessel function.

### 2.2.2. High-Pressure Hydrogen Gas Permeation Test (HPHP) Method

In the early exploration of gas permeability, Barrer et al. [16,17] used a differential pressure method. This method is to place a sample between a high-pressure chamber and a low-pressure chamber. According to the amount of the gas permeating from the high-pressure chamber to the low-pressure one, various coefficients of gas permeation are analyzed. At present, the HPHP test method, based on this principle, is optimized and improved by combining ASTM 1434 and ISO 7229 standards. During the test, under the condition of ensuring the stability of the hydrogen pressure on the high-pressure side, the change in the amount of hydrogen permeating through the sample over time should be recorded by a gas chromatograph, and an integrated transmission curve should be prepared.

When the amount of hydrogen permeating through the sample per unit time reaches a steady state, the permeation coefficient can be obtained by Equation (2). The diffusion coefficient  $D$  can be obtained based on the delay time  $\theta$  (Extrapolating the linear portion that the amount of hydrogen permeating through the sample per unit time at steady state in the reverse direction, the value of the intersection point with the time axis is that of  $\theta$ ) using Equation (3). The solubility coefficient  $S$  is determined by using the relationship among the three coefficients, as shown in Equation (4).

$$P = \frac{273.15 \times V \times l}{A \times \Delta p \times T \times 0.0227} \quad (2)$$

where  $l$  is the thickness of the sample (m),  $V$  is the amount of hydrogen permeating through the sample per unit time at steady state ( $\text{cm}^3/\text{s}$ ),  $A$  is the permeation area ( $\text{m}^2$ ),  $\Delta p$  is the pressure difference between the two sides of the sample (Pa), and  $T$  is the temperature (K).

$$D = \frac{l^2}{6\theta} \quad (3)$$

$l$  is the thickness of the sample (m),  $\theta$  is the delay time (s).

$$S = \frac{P}{D} \quad (4)$$

### 2.2.3. TDA Method versus HPHP Method

TDA and HPHP are two widely recognized test methods. In comparison, each one has its own advantages and disadvantages. From the aspect of the experimental equipment and test conditions, the TDA method at a non-steady state is relatively simple, and the experimental data can be obtained more easily and quickly. However, to ensure the constant

test pressure, the HPHP method requires a series of complex experimental equipment, and it is very difficult to continuously test and obtain data under high-pressure conditions. In terms of the accuracy of the experimental data, HPHP is indeed better, because it almost minimizes the error of hydrogen permeation under high pressure. This conclusion has been confirmed by the literature [12] and the result is shown in Figure 3. The numbers in the plot show the exposed pressure (ex. ① = 10 MP, ⑨ = 90 Mpa) and in brackets show the quantitative value of destruction. Figure 3a shows that there is little difference between the two methods when measuring the amount of penetrated hydrogen under low-pressure test conditions, but the result is just the reverse under a high-pressure environment. As the test pressure increases, the quantitative value of destruction of the sample also increases significantly. In addition, Figure 3b shows that no matter what material we use, the permeability coefficient measured by TDA is always larger than that of HPHP.

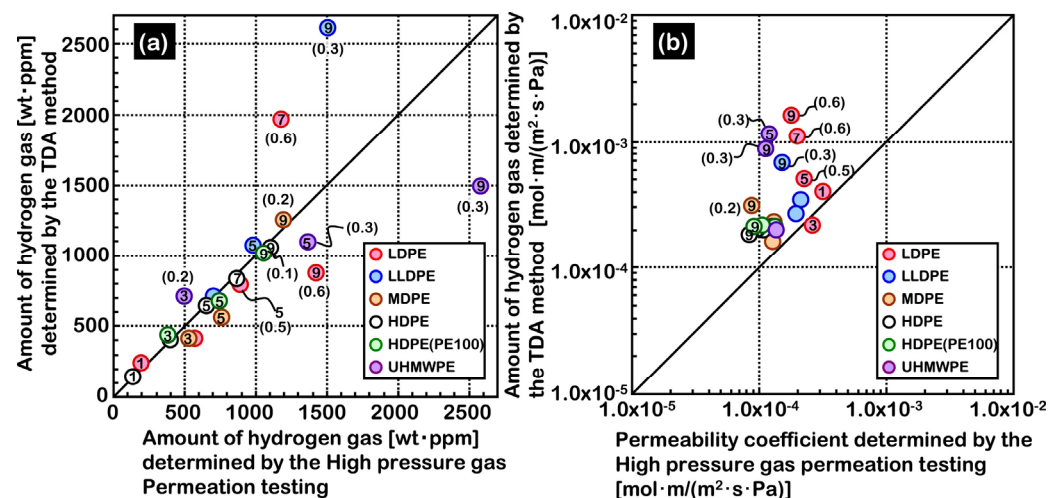


**Figure 3.** Comparison between HPHP method and TDA method: (a) Amount of penetrated hydrogen gas (b) Permeability, reproduced with permission from [12].

For the TDA method, the reason why the experimental data are biased and the measured value is always too large is mainly because the sample is damaged on the micro view [12]. In a high-pressure environment, the sample has absorbed enough hydrogen. When the decompression operation is performed, the gas inside the sample, for the reason that its diffusion rate is much lower than the decompression rate, will become supersaturated and accumulate in the microscopic voids (defects) in the material to cause stress concentration. When the stress or strain here exceeds the tear standard of the material, irreversible damage occurs. The damage caused by this reason is considered to be one of the failure behaviors of the liner material, and many scholars have described and explored this phenomenon [18,19]. At present, this is also an important direction of research on the liner material of type IV hydrogen storage tanks.

### 3. Factors Affecting Hydrogen Permeability

Hydrogen does not dissociate in polymers as it is known to do in metals, it exists in the form of diatomic molecules. Compared with other gas molecules, hydrogen has a smaller molecular dynamic diameter (about 2.8 Å), which makes it easier to diffuse inside the polymer. Good gas barrier property is one of the necessary properties of high-pressure hydrogen storage tanks, which is essential to the safety of on-board hydrogen. However, the permeability of gas in polymers is affected by many factors, such as temperature, pressure, etc. At present, only a small number of experts and scholars have researched this, and there are few related references. Generally, the permeability of gas in polymers is mainly affected by external conditions (such as temperature [20,21], pressure [15,22]), material properties (such as crystallinity [23,24], fillers [25,26], etc.), and the interaction between gas and material [27,28].

### 3.1. External Conditions

#### 3.1.1. Temperature

When using a hydrogen dispenser to fill the on-board type IV hydrogen storage tank with hydrogen, the gaseous hydrogen fuel is usually pre-cooled to 233 K (−40 °C) to prevent the temperature in the hydrogen storage tank from being too high during the filling process. At present, the application temperature range of the on-board hydrogen storage tank is between 233 K (−40 °C) and 358 K (85 °C) [29], so it is of great significance to explore the permeation law in such a situation. Barth et al. [21] summarized the temperature dependence of hydrogen permeability of various polymer materials (such as high-density polyethylene, polyamide, butyl rubber, etc.). When analyzing the influence of temperature, the permeation of hydrogen in polymer materials at different temperatures is plotted, as shown in Figure 4. Among all materials tested, polyamides and polyethylene show excellent gas barrier properties. Moreover, the hydrogen permeability coefficient of all materials increases as the temperature goes up. This phenomenon is known as Arrhenius's laws.

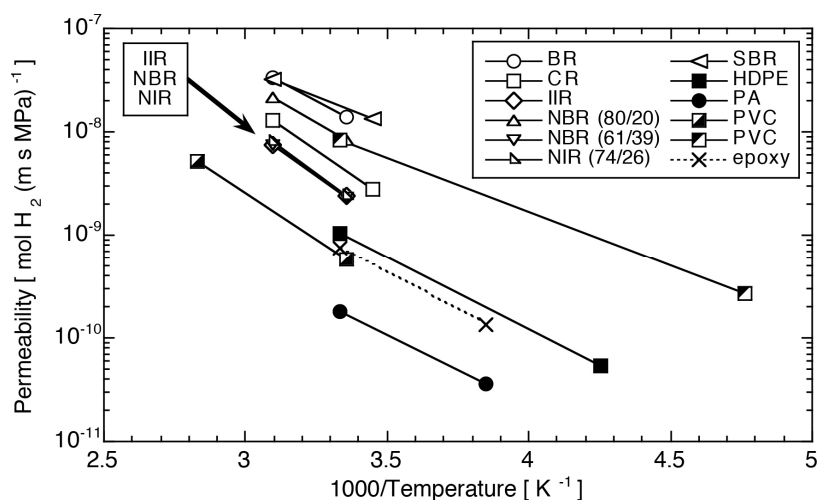


**Figure 4.** Temperature dependence of hydrogen permeability of various polymer materials, reproduced with permission from [21].

In fact, under a given pressure, many references exploring the influence of temperature on the gas permeability coefficient  $P$ , diffusion coefficient  $D$ , and solubility coefficient  $S$  in polymers have proved that the variation of the coefficients obeys Arrhenius's laws in a narrow temperature range [20,30]:

$$P(T) = P_0 \exp\left(-\frac{E_P}{RT}\right) \quad (5)$$

$$D(T) = D_0 \exp\left(-\frac{E_D}{RT}\right) \quad (6)$$

$$S(T) = S_0 \exp\left(-\frac{\Delta H_S}{RT}\right) \quad (7)$$

where  $P_0$ ,  $D_0$ , and  $S_0$  represent the limit values of various transportation coefficients when the temperature tends to infinity.  $E_P$ ,  $E_D$ , and  $\Delta H_S$  respectively, represent the apparent activation energy of the permeation process and diffusion process, and the heat of dissolution required for the penetrant to dissolve in the polymer matrix. It is obvious from the relationship of  $P = D \times S$  that  $E_P = \Delta H_S + E_D$ . For hydrogen, both  $E_D$  and  $\Delta H_S$  are positive values [31]. Therefore, it can be seen that under a certain pressure, as the temperature increases, the permeability of hydrogen in the polymer gradually increases, which is consistent with the trend shown in Figure 4.

### 3.1.2. Pressure

In the early research on gas permeability in the pipeline, Klopffer et al. [32] explored the permeability of pure gas and mixed gas (methane, carbon dioxide, hydrogen) in PE80 at a low experimental pressure of 0–20 bar (2 MPa). The experimental results did not show any effect of the applied pressure on the gas permeability, which was consistent with the phenomenon pointed out in the 2005 EHEC and 2006 WHEC meetings. This phenomenon also appears in Naito et al.'s research on the hydrogen permeability of LDPE [33]. Even at an experimental pressure as high as 80 bar (8 MPa), there is almost no change in the hydrogen permeability coefficient. However, the current hydrogen storage pressure of the on-board type IV hydrogen storage tank can reach 70 MPa. During the filling and using process, the allowable pressure needs to reach 1.25 times the nominal pressure; that is, 87.5 MPa [29], which is nearly 9 times higher than the previous experiment pressure. Thus, these phenomena cannot satisfy the description of hydrogen permeation in the type IV hydrogen storage tanks.

In order to explore the hydrogen permeability of polymers in a high-pressure environment deeply, Fujiwara et al. [15] developed a 90 MPa hydrogen permeability measurement system with high accuracy based on the principle of the HPHP method. Then they used it to evaluate the hydrogen permeability of HDPE. At a temperature of 30 °C, the effect of the applied pressure on different coefficients is shown in Figure 5. Experiments show that the amount of permeated hydrogen goes up with the increasing pressure, but the rate of increase gradually decreases. Furthermore, the permeability coefficient, diffusion coefficient, and solubility coefficient all decrease to different extents when the pressure increases. The variation value of the diffusion coefficient, shown in Figure 5, is slightly larger than that of the solubility coefficient, which proves that at a certain temperature, hydrogen permeation is mainly affected by diffusion rather than solubility. This phenomenon is completely different from the previous conclusions under low pressure. In addition, Figure 6 shows that the amount of penetrated gas per unit mass of HDPE increases as the test pressure increases, but the ratio of increase slows slightly. The deviation of the experimental curve from the dotted line reveals that the process of gas permeation does not obey Henry's law (a linear relation between the penetrant concentration in the polymer and its partial pressure) at high pressure. This is consistent with the previous research conclusions of Li et al. [34] on gas solubility. The movement and diffusion of the penetrant are considered to occur in the free volume (free volume is defined as the unoccupied region contained in the polymer volume, which can be obtained by the movement of polymer chain segments [24]). Thus, Barth et al. [21] attributed this deviation to the hydrostatic effect, which will reduce the free volume in polymers, inhibit the process of diffusion, and reduce the permeability coefficient. At the same time, literature [35] shows that the crystallinity of polyethylene (the crystallized region can inhibit gas diffusion) under a high-pressure hydrogen environment has a certain degree of increase, thereby inhibiting diffusion. However, this change is reversible and it returns to the original crystallinity when the pressure is reduced to atmospheric pressure. Pressure changing with time may affect the properties of polymers or even leads to the failure of certain properties of polymers. Therefore, further measurements are needed for such a situation.

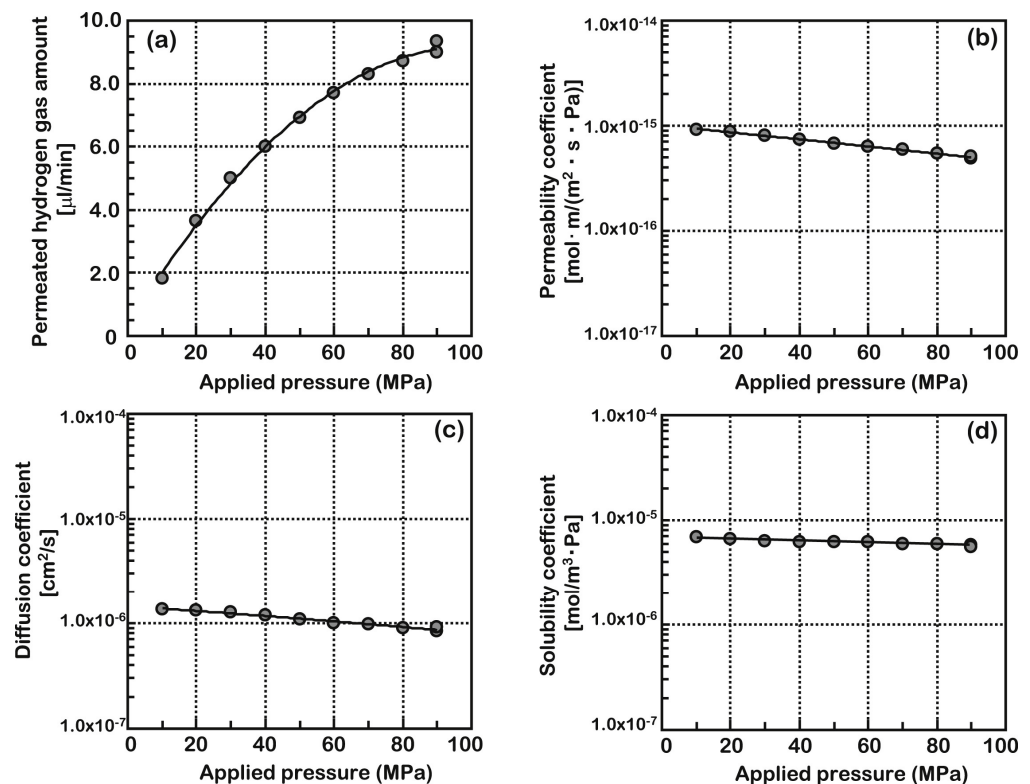


**Figure 5.** Pressure dependence of the permeation coefficients, reproduced with permission from [15]: (a) the amount of hydrogen permeation; (b) the permeability coefficient; (c) the diffusion coefficient; (d) the solubility coefficient.

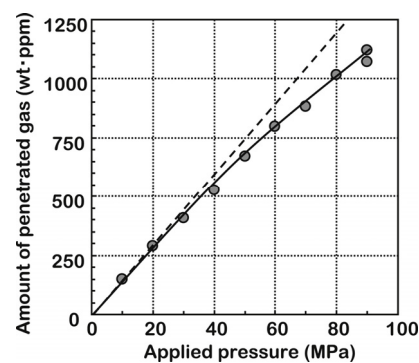


**Figure 6.** Hydrogen permeation per unit mass of HDPE at different pressures, reproduced with permission from [15].

### 3.2. Material Properties

Many scholars have explored the permeability of different materials to the same gas [19,35], which is of great significance to the selection of suitable materials with strong gas barrier properties. When deeply exploring specific influencing factors, it may be caused by some internal structural factors (such as crystallinity, fillers, etc.) for polymer materials.

#### 3.2.1. Crystallinity and Molecular Chain

When measuring the hydrogen permeability of perfluorosulfonic acid polymer (PFSA) membranes, Takeuchi et al. [23] experimentally observed that the transmission of hydrogen was limited by the crystallinity of the polymer. Higher crystallinity reduces the volume fraction of cavities in the polymer and increases the gas barrier properties of the film. Coincidentally, Kane [24] also demonstrated the influence of crystallinity in polyethylene

on hydrogen permeability through calculations and found that the higher the crystallinity, the stronger the barrier to gas transmission.

Polyamide is a semi-crystalline polymer that generally has a lower crystallinity than high crystallinity materials such as polyethylene. According to the crystallinity, the gas barrier properties of polyethylene should be stronger than that of polyamide. Interestingly, under the same experimental conditions, Klopffer et al. [28] found that the hydrogen permeability of PE100 with a crystallinity of 60% was actually higher than that of PA11 with a crystallinity of 20% ( $8.93 \times 10^{-16}$  mol/(Pa·m·s) for PE100 and  $3.57 \times 10^{-16}$  mol/(Pa·m·s) for PA11 at 20 °C and 2 MPa). This phenomenon has also appeared in the research of other scholars [36,37]. This shows that the factors affecting the gas permeability of polymer are far more than crystallinity, and may be related to the cohesive energy density of the amorphous phase [28]. This is because there are polar structures in polyamide materials that can form intermolecular and intramolecular hydrogen bonds, which enhance the interaction between molecular chains and reduce permeability [38]. Due to hydrogen bonds, Pepin et al. [39] found that the hydrogen permeability coefficient of PA12 is 5 times that of PA6, as high as  $3.42 \times 10^{-15}$  mol/(Pa·m·s), under the conditions of 55 °C and 18 MPa. Moreover, the side chain groups of the molecular chain in the polymer and the orientation of the molecular chain also influence the gas permeability to a certain extent. The former affects the movement of molecular chains in the polymer, while the latter is related to the way the polymer is formed. Smith [40] explored the durability and hydrogen permeability of polymers such as HDPE and PA made by different molding methods during temperature cycling experiments. The specific experimental conditions and results are shown in Table 1. The result shows that various molding methods have a certain effect on the hydrogen permeability of polymers (the hydrogen permeability of injection-molded HDPE is higher than that of extrusion-molded), however, the effect is not statistically significant.

**Table 1.** Relationship between molding methods and hydrogen permeability of polymers [40].

Molding Methods	Polymer	Experimental Conditions		Comparison of Results (P)
		Temperature Range (°C)	Pressure (Bar)	
Injection-molded	HDPE	−30~85	about 135	P (Injection-molded HDPE)>
Extrusion-molded	HDPE			P (Extrusion-molded HDPE)≈
Extrusion-molded	PA6			P (Extrusion-molded PA6)>
Compression-molded	TLCP			P (Compression-molded TLCP
Blow-molded	PET			Blow-molded PET

### 3.2.2. Additives

In the actual manufacturing process, various substances are often added to modify the polymer to meet the various properties that we need. These substances such as crosslinking agents, plasticizers, and fillers will affect the gas barrier properties of the polymer.

The addition of crosslinking agent will change the degree of cross-linking between molecular chains, affect the gaps between molecular chains and then affect the penetration of gas molecules. The higher the degree of crosslinking, the more difficult it is for molecular chains to move and for penetrants with a diameter larger than the cross-linking gap to diffuse. The influence of plasticizers on gas transmission has been reported in the literature [13]. At 120 °C and 4 MPa pressure, Flaconnèche et al. [41] explored the influence of different mass fractions (0%, 7.5%, 12.5%, 19%, 29.5%) of plasticizers on the gas transmission performance of PA11 and found that the gas diffusion coefficient is slightly modified by the content of the plasticizer, but has almost no effect on solubility coefficient. The reason may be that the addition of plasticizers weakens the interaction between polymer molecular chains in the amorphous phase and gives the macromolecular chains more freedom to move, which is conducive to the diffusion of gas molecules [13].

Adding the fillers (usually an inorganic substance) directly to the polymer is the simplest way to improve its gas barrier properties. The addition of fillers will form a physical

barrier in the polymer, which will make the gas transmission path more complicated. This phenomenon is called the “tortuous effect”, as shown in Figure 7.

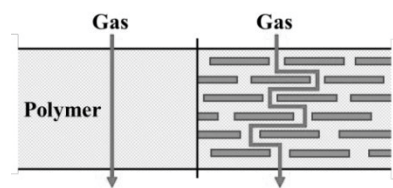


Figure 7. The “tortuous effect”, reproduced with permission from [25].

The influence of the “tortuous effect” has been proved by Klopffer et al. [42]. The gas barrier properties of both PA11 and PE100 were improved to different extents after modification. However, the specific filling effect will be complicated due to the various properties of the filler, such as type and shape. In the research on the shape of fillers, literature [43,44] explored the influence of filler shape (the aspect ratio), content, and other factors on the gas barrier properties of polymers, and used a mathematical equation to express the law:

$$P_{rel} = \frac{P}{P_0} = \left(1 + \mu \frac{\alpha^2 \phi^2}{1 - \phi}\right)^{-1} \quad (8)$$

where  $P/P_0$  represents the ratio of polymer permeability coefficient after filling to before filling, and  $\mu$ ,  $\alpha$ , and  $\phi$  represent geometric factor, aspect ratio, and volume fraction related to the filling, respectively.

According to this rule, Habel et al. [26] used NaHec with a large aspect ratio as the nanofiller and optimized its arrangement in the polymer to produce a lightweight ultra-high barrier liner for helium and hydrogen. Sun et al. [45] comprehensively investigated the hydrogen permeability of PA6 filled with lamellar inorganic components (LIC). The result showed that the hydrogen permeability of LIC/PA6, under various temperatures (10 °C, 25 °C, 85 °C) and pressure (25 MPa, 35 MPa, 50 MPa) conditions, was decreased by 3–5 times than the pure PA6. The maximum permeability coefficient of the LIC/PA6 they measured is  $6.10 \times 10^{-16}$  mol/(Pa·m·s) which was lower than  $1.24 \times 10^{-15}$  mol/(Pa·m·s) required by the gas cylinder standard. However, the optimal addition ratio of LIC still needs to be explored. In addition, there are many research studies and applications on the “tortuous effect” of fillers [46,47].

### 3.3. Interaction between Gas and Material

When the permeated gas interacts with the polymer, part of the properties of the polymer will be changed, which may affect the gas permeation process. For example, many studies have shown that carbon dioxide can easily plasticize polymers [48,49], which affects the properties of polymers. Based on this, some scholars have also studied the interaction between hydrogen and materials.

In an environment with a hydrogen pressure of 3 MPa, Castagnet et al. [27] conducted a series of mechanical tests (tensile, creep, ductile fracture, etc.) on PE and PA11, which showed that the transmission of hydrogen had no obvious effect on the amorphous and crystalline phase of the material, and the influence on the mechanical experiment results of materials does not exceed 10%. In other studies under low pressure [24,28], no obvious hydrogen effect was found. Subsequently, Fujiwara et al. [12] also proved that this effect was not obvious under high pressure, which is consistent with the literature [15]. However, there are almost no experimental data that measured at both high pressure and high temperature and this needs to be further studied.

## 4. Prediction Models

In order to describe the transport behavior of gas in polymers in more detail and predict the permeation behavior of gas, many theoretical models have been proposed. Although most of these models are summarized based on the diffusion behavior of gases

such as CO<sub>2</sub> and CH<sub>4</sub> in polymers, they can still be used as a reference for predicting the permeation behavior of hydrogen. Due to various factors, these expressions in these models become extremely complicated.

#### 4.1. Dual-Mode Sorption Model

This model was first proposed by Barrer et al. [50], and it can accurately describe the dissolution and diffusion of gas or vapor in glassy polymers in a simple way. In this model, the penetrant molecules are divided into two groups: one group is the penetrant molecules dissolved in the polymer by Henry's law with a concentration of  $C_D$ , and the other is adsorbed at a specific site (holes or microvoids) by Langmuir-Mode with a concentration of  $C_H$ . There is a local balance between the two parts of the penetrant. The total concentration can be expressed by Equation (9) under the equilibrium pressure  $P$ :

$$C = C_D + C_H = k_D p + \frac{C'_H b p}{1 + b p} \quad (9)$$

where  $k_D$ ,  $b$ , and  $C'_H$  are three constants [51,52], which are Henry's law constants (representing the solubility of the gas in polymers), Langmuir hole affinity parameters (representing affinity for sites), and Langmuir capacity Parameter (a measure of the concentration in "holes").

In this model, the two groups of penetrant molecules have their own diffusion coefficients  $D_D$  and  $D_H$ . The penetrant molecules are more likely to diffuse in the environment of Henry's population, thus,  $D_D$  is generally greater than  $D_H$ , that is,  $F = D_H/D_D \leq 1$ . Assigning different values to the physical parameter  $F$  can make the model have different practical meanings. Koros et al. [53,54] believe that all the penetrant molecules dissolved in the polymer by Henry's law can move, while only part of the penetrant molecules at a specific site can do. Therefore, the concentration of permeate gas that can actually move is  $C_D + F C_H$ . Combined with Equation (10), the permeability coefficient and time lag of the penetrant are expressed as follows:

$$S = \frac{C}{p} \quad (10)$$

$$P = DS = k_D D_D \left( 1 + \frac{FK}{1 + b p} \right) \quad (11)$$

$$\theta = \frac{l^2}{6D_D} [1 + f(K, F, b, p)] \quad (12)$$

where  $K = C'_H b / k_D$ .  $f$  is a complicated function. Although  $k_D$ ,  $D_H$  and  $D_D$  are considered as three constants in this model, the solubility and diffusion coefficient will be affected as the pressure changes continuously. In addition, the exponential correlation between  $D$  and concentration can be introduced to describe the strong interaction between the penetrant and polymers [55]. However, the properties and distribution of the micropores in this model are not very clear, and there is a difference between the parameters used for sorption and those required to describe desorption. Moreover, significant errors may be caused when using existing parameters for extrapolation calculations [56].

#### 4.2. Gas-Polymer Matrix Model

In this model, it is assumed that there is an interaction between the penetrant molecules and the polymer matrix, which affects the internal structural properties of the polymer and promotes the frequency of molecular chain movement [13,57]. The penetrant molecules existing between the polymer molecular chains reduce the activation energy required to separate the chains, and the mobility of the chain segments is enhanced. The specific influence on the solubility and gas diffusion can be expressed by the following equations:

$$S = S_0 \exp(-\alpha^* \kappa) \quad (13)$$

$$D = D_0(1 + \beta^* \kappa) \exp(\beta^* \kappa) \quad (14)$$

$$\kappa = \frac{T_g(0) - T_g(C)}{T} \quad (15)$$

It is worth noting that the solution of the diffusion coefficient is generalized from the solubility solution theory.  $S_0$  and  $D_0$  respectively, represent the limit values of solubility and diffusion coefficient at zero concentration,  $\alpha^*$  and  $\beta^*$  are constants, and  $T_g(0)$  and  $T_g(C)$  represent the glass transition temperatures of pure polymers and that of gas-polymer systems. When it is assumed that the glass transition temperature  $T_g$  decreases linearly as the concentration increases [58], there is also a linear relationship between  $\kappa$  and the concentration  $C$  on the upstream side of the membrane, the Equation (13) and Equation (14) can be rewritten as

$$S = S_0 \exp(-\alpha C) \quad (16)$$

$$D = D_0(1 + \beta C) \exp(\beta C) \quad (17)$$

where  $\alpha$  and  $\beta$  are constants. When the coefficient  $\beta C$  is very small, the permeability coefficient and time lag of the penetrant are expressed as Equation (18) and Equation (19) [59]. Contrary to the dual-mode sorption model, the time lag values calculated by this model are in good agreement with the experimental results [13].

$$P = D_0 S_0 \exp[(\beta - \alpha)C] \quad (18)$$

$$\theta = \frac{l^2}{6D_0} \frac{10 + 25\beta C + 16(\beta C)^2}{10(1 + \beta C)^3} \quad (19)$$

#### 4.3. Nonequilibrium Lattice Fluid Thermodynamic Model

The nonequilibrium lattice fluid thermodynamic (NELF) model is obtained by applying the nonequilibrium thermodynamics for the glassy polymer (NET-GP) to the lattice fluid (LF) model. From the perspective of thermodynamics, it can precisely describe the different behaviors of the penetrant molecules in the experiment relying on the nonequilibrium chemical potential of the substances in the polymer mixture. Moreover, the validity and accuracy of the model have been proved in the calculation and prediction of the solubility isotherms of pure glassy polymer and mixed gas [60,61]. In this model, the diffusion coefficient is composed of the product of the kinetic factor and the thermodynamic factor:

$$D = L \frac{\partial \mu_1 / RT}{\partial \ln \omega_1} \equiv L \alpha \quad (20)$$

$$L = L_0 e^{(\beta \omega_1)} \quad (21)$$

$L$  is a kinetic factor, also known as mobility, and its value is related to the resistance encountered in the transport of penetrant molecules. In order to avoid the application of a large number of parameters, the expression is simplified as much as possible. For the expression of mobility, an exponential expression conforming to the migration experience of penetrant molecules is adopted, as shown in Equation (21).  $L_0$  and  $\beta$  represent the infinite dilution mobility coefficient and the plasticization coefficient, respectively. These two adjustable parameters can be obtained from the instantaneous adsorption diffusion data or steady-state permeability data.  $\omega_1$  represents the mass fraction of penetrant molecules 1 dissolved in polymer 2 (subscript 1 usually represents gas solute, subscript 2 represents polymer). For the thermodynamic factor  $\alpha$  without any adjustable parameters, its specific

value can be obtained directly from the solubility isotherm or indirectly calculated by the nonequilibrium thermodynamics of the glassy polymer in the NELF model [62]:

$$\frac{\mu_1^{NE}}{RT} = \ln\left(\frac{\omega_1\rho_2}{\omega_2\rho_1^*}\right) - \frac{M_1 p_1^*}{\rho_1^* RT_1^*} \left\{ \begin{aligned} & \left[ 1 + \left( \frac{T_1^* p_1^*}{T_1^* p_1^*} - 1 \right) \frac{\omega_2 \rho_2^*}{\rho_2} \right] \ln\left( 1 - \frac{\rho_2}{\omega_2 \rho_2^*} \right) + \\ & \frac{T_1^* p_1^*}{T_1^* p_1^*} + \frac{\rho_2}{\omega_2 \rho_2^*} \left[ \frac{T_1^*}{T} \left( 1 + \frac{p_1^*}{p_1^*} - \left( \frac{\rho_2}{\omega_2 \rho_2^*} \right)^2 \frac{\Delta p_{12}^*}{p_1^*} \right) \right] \end{aligned} \right\} \quad (22)$$

$$\Delta p_{12}^* = p_1^* + p_2^* - 2(1 - k_{12} \sqrt{p_1^* p_2^*}) \quad (23)$$

$\rho_2$  is the nonequilibrium density of the polymer, and  $k_{12}$  is the binary interaction parameter between the penetrant molecule and the polymer.  $M_1$ ,  $T_1^*$ ,  $P_1^*$  and  $\rho_1$ , respectively, represent the molar mass, characteristic temperature, pressure, and density of penetrant molecules. The characteristic properties  $T^*$ ,  $P^*$ , and  $\rho^*$  of the penetrant–polymer mixture can be calculated by referring to the mixing rules proposed by Sanchez and Lacombe [63], and some of the specific characteristic values can refer to the experimental data in other literature [64,65] or select from the literature [66]. When the gas penetration reaches a steady state, the following equation should be met:

$$J_1 l = M_1 \dot{N}_1 l = - \int_{\omega_1^u}^{\omega_1^d} \rho D d\omega_1 = \int_{\omega_1^d}^{\omega_1^u} \rho L_0 e^{\beta\omega_1} \alpha d\omega_1 \quad (24)$$

where  $J_1$  represents the mass flux of the penetrant.  $N_1$ ,  $\rho$ ,  $l$  are the steady-state molar flux of the penetrant, the density of the polymer, and the thickness of the polymer, respectively. The superscripts  $u$  and  $d$  represent the upstream and downstream sides of the polymer membrane, respectively.

Concerning the phase equilibrium conditions, the expression of steady-state permeability coefficient can be derived:

$$P_1 = \frac{1}{M_1 (p_1^u - p_1^d)} \int_{p_1^d}^{p_1^u} \rho L_0 e^{\beta\omega_1} \frac{\omega_1}{p_1} z_1 dp_1 \quad (25)$$

$p_1^u$  and  $p_1^d$  represent the pressure on the upstream and downstream sides of the polymer membrane, and  $z_1$  is the gas compression factor (calculated by the Peng–Robinson equation of state). The value of  $\frac{\omega_1}{p_1}$  can be obtained from the solubility isotherm and the meaning of other parameters will not be repeated here. Without adding adjustable parameters, the NELF model describes the process of gas permeation in detail even in the case of plasticization and has both simplicity and intuitiveness.

#### 4.4. Free Volume Theory

The free volume theory plays a pivotal role in the study of high molecular polymers and can explain many phenomena and principles. For example, for the two adjustable parameters  $L_0$  and  $\beta$  in the NELF model, the free volume can also be used to characterize the correlation [67]. In this theory, the volume of an object is divided into occupied volume (Van der Waals, refer to the literature [68] for specific calculations) and free volume. The transport of penetrant molecules in the polymer depends on the redistribution of free volume [69] which means only when the free volume around the penetrant molecules reaches or exceeds a certain critical value, the penetrant molecules can move. The free volume fraction of a polymer can be expressed as the ratio of free volume to the total volume, and the free volume fraction of the relevant system is given by the following equation (subscript 1 usually represents gas solute, subscript 2 represents polymer):

$$f = \phi_1 f_1 + \phi_2 f_2 \quad (26)$$

where  $\phi_1$ ,  $f_1$ ,  $\phi_2$ , and  $f_2$  are the volume fraction and free volume fraction of penetrant molecules and polymers in the system, respectively. For the expression of the diffusion coefficient, the theory gives the following expression [70,71]:

$$D_T = RTA_d \exp\left(\frac{-B_d}{f}\right) = RTm_d \quad (27)$$

where  $A_d$ ,  $B_d$ , and  $m_d$  respectively, represent the parameters related to the external dimensions of the penetrant molecules, the characteristic parameters related to the available free volume fraction, and the mobility of the penetrant molecules. In addition, Equation (27) can also be expressed as

$$D_T = A \exp\left(\frac{-bv^*}{f}\right) \quad (28)$$

where  $A$  and  $b$  are constants related to the system and  $v^*$  is the critical volume of penetrant molecules.

Combining the entropy of the mixture and the Flory–Huggins equation [72], the solubility of the penetrant in the polymer can be described as

$$S = \frac{f}{f_1 p_1^0 \exp(1 + \chi_1)} \approx \frac{f_2}{f_1 p_1^0 \exp(1 + \chi_1)} = kf_2 \quad (29)$$

where  $p_1^0$  is the saturated vapor pressure of the penetrant at temperature  $T$  and  $\chi_1$  is the Flory–Huggins interaction parameter.  $f_2$  can be used directly instead of  $f$  when assuming that the value of  $\phi_1$  is very small. Then the entire equation is simplified.  $k$  is considered a constant in the system.

For semi-crystalline polymers such as polyamides, gas transport only occurs in the amorphous phase region and has nothing to do with the crystallized region [24]. Therefore, the previous equations should be rewritten as

$$S_a = kf_a \quad (30)$$

$$D_{Ta} = A \exp\left(\frac{-bv^*}{f_a}\right) \quad (31)$$

$$f_a = \frac{v - v_0}{v} \quad (32)$$

The subscript  $a$  represents that these coefficients are related to the amorphous phase region.  $v$  and  $v_0$ , respectively, represent the total volume and occupied volume of the amorphous phase region (Van der Waals). Concerning the relationship among the permeability coefficient, solubility coefficient, and diffusion coefficient, the permeability coefficient of the penetrant in polymers can be expressed as Equation (33). However, when the temperature is higher than the glass transition temperature, the free volume fraction of polymers will change, which may make the calculation more complicated.

$$P = D_{Ta} S_a = kf_a A \exp\left(\frac{-bv^*}{f_a}\right) \quad (33)$$

## 5. Conclusions

In the field of HFCVs, the type IV hydrogen storage tank, for its low cost, lightweight, and low storage energy consumption, has become a research hotspot. However, hydrogen permeation will occur inevitably for the use of polymers. It is very essential and challenging to reduce the hydrogen permeation amount as much as possible and predict the permeation behavior, which will still be the focus of future research. In this paper, the process of hydrogen permeation and test methods (TDA and HPHP) are firstly discussed in detail. Comparing the two methods, it is found that the HPHP method is more suitable for the measurement of hydrogen permeation amount under high-pressure conditions. This paper

then analyzes the factors that affect the process of hydrogen permeation and the barrier mechanism of the liner material and summarizes the prediction models of gas permeation. This can not only improve our understanding of the hydrogen permeation mechanism but also provide a reference for following-up researchers and research on the safety of HFCVs.

To date, the permeation of hydrogen in various polymers has been explored from various aspects such as external conditions, material properties, and the interaction between gases and materials. However, these studies are not comprehensive and mature compared with other gas permeation studies. From the perspective of on-board hydrogen safety, there are still many things that need to be further studied:

1. Although the factors and rules of most gas permeation in polymers have been summarized, these rules are rarely concluded based on the hydrogen permeation in the liner materials (such as HDPE and polyamide, etc.) of the on-board type IV hydrogen storage tank. Therefore, this can only be regarded as a universal law and there is still a lack of systematic research on hydrogen permeation in the material of the on-board type IV hydrogen storage tank.
2. The pressure in the type IV hydrogen storage tank is as high as 700 bar. Most of the experiments were carried out at low pressure and the hydrogen permeation data under high pressure is insufficient. In addition, there is no special experimental study on the plasticization of the liner material of the hydrogen storage tank in the high-pressure hydrogen environment, and no detailed evaluation of its physical and mechanical properties in a high-pressure hydrogen environment.
3. Based on the high-pressure hydrogen permeation data, the prediction model needs to be further optimized and improved to ensure its accuracy and predictive ability in the description of permeation phenomena in a high-pressure environment.
4. When polyamide is used as the liner material of the type IV hydrogen storage tank, the amine group and carbonyl group contained in the molecular chain will make the material have water absorption. The degree of water absorption of the material will lead to changes in many properties, so the influence of humidity on polyamide materials cannot be ignored.

The harsh working conditions of the on-board high-pressure type IV hydrogen storage tank (the working temperature is between 233 K (−40 °C) to 358 K (85 °C) and the allowable pressure needs to be 1.25 times the nominal pressure, which is 87.5 MPa) will impose stricter requirements on the liner material of the hydrogen storage tank. Both temperature and pressure will show continuous changes (the change is particularly drastic when filling) in the practical application of the tanks. How these changes affect the gas barrier properties of the liner material and how to model are also issues worthy of further study in the future.

**Author Contributions:** Conceptualization, Y.S., H.L., W.Z. and C.Z.; investigation, Y.S.; resources, H.L., W.Z. and C.Z.; writing—original draft preparation, Y.S.; writing—review and editing, Y.S. and H.L.; visualization, Y.S.; supervision, H.L.; project administration, H.L. and Y.S.; funding acquisition, H.L., W.Z. and C.Z. All authors have read and agreed to the published version of the manuscript.

**Funding:** This research was funded by the National Key Research and Development Program of China, grant number 2017YFB0102804.

**Conflicts of Interest:** The authors declare no conflict of interest.

## References

1. References Al-Juboori, O.; Sher, F.; Hazafa, A.; Khan, M.K.; Chen, G.Z. The effect of variable operating parameters for hydrocarbon fuel formation from CO<sub>2</sub> by molten salts electrolysis. *J. CO<sub>2</sub> Util.* **2020**, *40*, 101193. [[CrossRef](#)]
2. Al-Shara, N.K.; Sher, F.; Iqbal, S.Z.; Curnick, O.; Chen, G.Z. Design and optimization of electrochemical cell potential for hydrogen gas production. *J. Energy Chem.* **2021**, *52*, 421–427. [[CrossRef](#)]
3. Al-Shara, N.K.; Sher, F.; Iqbal, S.Z.; Sajid, Z.; Chen, G.Z. Electrochemical study of different membrane materials for the fabrication of stable, reproducible and reusable reference electrode. *J. Energy Chem.* **2020**, *49*, 33–41. [[CrossRef](#)]
4. Sher, F.; Al-Shara, N.K.; Iqbal, S.Z.; Jahan, Z.; Chen, G.Z. Enhancing hydrogen production from steam electrolysis in molten hydroxides via selection of non-precious metal electrodes. *Int. J. Hydrog. Energy* **2020**, *45*, 28260–28271. [[CrossRef](#)]

5. Al-Shara, N.K.; Sher, F.; Yaqoob, A.; Chen, G.Z. Electrochemical investigation of novel reference electrode Ni/Ni(OH)<sub>2</sub> in comparison with silver and platinum inert quasi-reference electrodes for electrolysis in eutectic molten hydroxide. *Int. J. Hydrog. Energy* **2019**, *44*, 27224–27236. [[CrossRef](#)]
6. Rivard, E.; Trudeau, M.; Zaghbi, K. Hydrogen Storage for Mobility: A Review. *Materials* **2019**, *12*, 1973. [[CrossRef](#)]
7. Balasooriya, W.; Clute, C.; Schrittmesser, B.; Pinter, G. A Review on Applicability, Limitations, and Improvements of Polymeric Materials in High-Pressure Hydrogen Gas Atmospheres. *Polym. Rev.* **2021**, *61*, 1–36. [[CrossRef](#)]
8. Mori, D.; Hirose, K. Recent challenges of hydrogen storage technologies for fuel cell vehicles. *Int. J. Hydrog. Energy* **2009**, *34*, 4569–4574. [[CrossRef](#)]
9. Barthelemy, H.; Weber, M.; Barbier, F. Hydrogen storage: Recent improvements and industrial perspectives. *Int. J. Hydrog. Energy* **2017**, *42*, 7254–7262. [[CrossRef](#)]
10. Pepin, J.; Laine, E.; Grandidier, J.C.; Benoit, G.; Mellier, D.; Weber, M.; Langlois, C. Replication of liner collapse phenomenon observed in hyperbaric type IV hydrogen storage vessel by explosive decompression experiments. *Int. J. Hydrog. Energy* **2018**, *43*, 4671–4680. [[CrossRef](#)]
11. Ahluwalia, R.K.; Hua, T.Q.; Peng, J.K. On-board and Off-board performance of hydrogen storage options for light-duty vehicles. *Int. J. Hydrog. Energy* **2012**, *37*, 2891–2910. [[CrossRef](#)]
12. Fujiwara, H.; Ono, H.; Ohyama, K.; Kasai, M.; Kaneko, F.; Nishimura, S. Hydrogen permeation under high pressure conditions and the destruction of exposed polyethylene-property of polymeric materials for high-pressure hydrogen devices (2)-. *Int. J. Hydrog. Energy* **2021**, *46*, 11832–11848. [[CrossRef](#)]
13. Klopffer, M.H.; Flaconneche, B. Transport properties of gases in polymers: Bibliographic review. *Oil Gas Sci. Technol.* **2001**, *56*, 223–244. [[CrossRef](#)]
14. Yamabe, J.; Nishimura, S. Influence of fillers on hydrogen penetration properties and blister fracture of rubber composites for O-ring exposed to high-pressure hydrogen gas. *Int. J. Hydrog. Energy* **2009**, *34*, 1977–1989. [[CrossRef](#)]
15. Fujiwara, H.; Ono, H.; Onoue, K.; Nishimura, S. High-pressure gaseous hydrogen permeation test method -property of polymeric materials for high-pressure hydrogen devices (1)-. *Int. J. Hydrog. Energy* **2020**, *45*, 29082–29094. [[CrossRef](#)]
16. Brubaker, D.W.; Kammermeyer, K. Flow of gases through plastic membranes. *Ind. Eng. Chem.* **1953**, *45*, 1148–1152. [[CrossRef](#)]
17. Van Amerongen, G.J. The permeability of different rubbers to gases and its relation to diffusivity and solubility. *J. Appl. Phys.* **1946**, *17*, 972–985. [[CrossRef](#)]
18. Lorge, O.; Briscoe, B.; Dang, P. Gas induced damage in poly (vinylidene fluoride) exposed to decompression. *Polymer* **1999**, *40*, 2981–2991. [[CrossRef](#)]
19. Stevenson, A.; Morgan, G. Fracture of elastomers by gas decompression. *Rubber Chem. Technol.* **1995**, *68*, 197–211. [[CrossRef](#)]
20. George, S.C.; Thomas, S. Transport phenomena through polymeric systems. *Prog. Polym. Sci.* **2001**, *26*, 985–1017. [[CrossRef](#)]
21. Barth, R.R.; Simmons, K.L.; San Marchi, C. *Polymers for Hydrogen Infrastructure and Vehicle Fuel Systems: Applications, Properties, and Gap Analysis*; Sandia National Laboratories: Albuquerque, NM, USA; Livermore, CA, USA, 2013. [[CrossRef](#)]
22. Klopffer, M.H.; Berne, P.; Espuche, E. Development of Innovating Materials for Distributing Mixtures of Hydrogen and Natural Gas. Study of the Barrier Properties and Durability of Polymer Pipes. *Oil Gas Sci. Technol.* **2015**, *70*, 305–315. [[CrossRef](#)]
23. Takeuchi, K.; Kuo, A.T.; Hirai, T.; Miyajima, T.; Urata, S.; Terazono, S.; Okazaki, S.; Shinode, W. Hydrogen Permeation in Hydrated Perfluorosulfonic Acid Polymer Membranes: Effect of Polymer Crystallinity and Equivalent Weight. *J. Phys. Chem. C* **2019**, *123*, 20628–20638. [[CrossRef](#)]
24. Kane, M. *Permeability, Solubility, and Interaction of Hydrogen in Polymers—An Assessment of Materials for Hydrogen Transport*; SRS: Aiken, SC, USA, 2008. [[CrossRef](#)]
25. Cui, Y.B.; Kundalwal, S.I.; Kumar, S. Gas barrier performance of graphene/polymer nanocomposites. *Carbon* **2016**, *98*, 313–333. [[CrossRef](#)]
26. Habel, C.; Tsurko, E.S.; Timmins, R.L.; Hutschreuther, J.; Kunz, R.; Schuchardt, D.D.; Rosenfeldt, S.; Altstadt, V.; Breu, J. Lightweight Ultra-High-Barrier Liners for Helium and Hydrogen. *ACS Nano* **2020**, *14*, 7018–7024. [[CrossRef](#)] [[PubMed](#)]
27. Castagnet, S.; Grandidier, J.C.; Comyn, M.; Benoit, G. Mechanical Testing of Polymers in Pressurized Hydrogen: Tension, Creep and Ductile Fracture. *Exp. Mech.* **2012**, *52*, 229–239. [[CrossRef](#)]
28. Klopffer, M.-H.; Berne, P.; Castagnet, S.; Weber, M.; Hochstetter, G.; Espuche, E. Polymer pipes for Distributing Mixtures of Hydrogen and Natural Gas. Evolution of Their Transport and Mechanical Properties after an Ageing under an Hydrogen Environment. In Proceedings of the World hydrogen energy conference: Building bridges to the hydrogen energy economy, Essen, Germany, 16–21 May 2010.
29. Maus, S.; Hapke, J.; Ranong, C.N.; Wuchner, E.; Friedlmeier, G.; Wenger, D. Filling procedure for vehicles with compressed hydrogen tanks. *Int. J. Hydrog. Energy* **2008**, *33*, 4612–4621. [[CrossRef](#)]
30. Rogers, C. Permeation of gases and vapours in polymers. In *Polymer Permeability*; Springer: Dordrecht, Holland, 1985; pp. 11–73.
31. Baker, R.W. *Polymer Permeability*; Comyn, J., Ed.; Elsevier Applied Science Publishers: London, UK, 1985; p. 383. ISBN 0-85334-322-5.
32. Klopffer, M.H.; Flaconneche, B.; Odru, P. Transport properties of gas mixtures through polyethylene. *Plast. Rubber Compos.* **2007**, *36*, 184–189. [[CrossRef](#)]
33. Naito, Y.; Mizoguchi, K.; Terada, K.; Kamiya, Y. The Effect of Pressure on Gas Permeation through Semicrystalline Polymers above the Glass-Transition Temperature. *J. Polym. Sci. Pol. Phys.* **1991**, *29*, 457–462. [[CrossRef](#)]
34. Li, N.; Long, R. Permeation through plastic films. *AIChE J.* **1969**, *15*, 73–80. [[CrossRef](#)]

35. Fumitoshi, K.K.O.; Hirota, F.; Shin, N. Influence of high-pressure hydrogen gas on crystalline polymers. In Proceedings of the 33rd Polymer Degradation Discussion Group, St Julians, Malta, 1–5 September 2019.
36. Humpenöder, J. Gas permeation of fibre reinforced plastics. *Cryogenics* **1998**, *38*, 143–147. [CrossRef]
37. Yersak, T.A.; Baker, D.R.; Yanagisawa, Y.; Slavik, S.; Immel, R.; Mack-Gardner, A.; Herrmann, M.; Cai, M. Predictive model for depressurization-induced blistering of type IV tank liners for hydrogen storage. *Int. J. Hydrog. Energy* **2017**, *42*, 28910–28917. [CrossRef]
38. Park, G.S.; Crank, J. *Diffusion in Polymers*; Academic Press: London, UK; New York, NY, USA, 1968.
39. Pepin, J.; Laine, E.; Grandier, J.C.; Castagnet, S.; Blanc-vannet, P.; Papin, P.; Weber, M. Determination of key parameters responsible for polymeric liner collapse in hyperbaric type IV hydrogen storage vessels. *Int. J. Hydrog. Energy* **2018**, *43*, 16386–16399. [CrossRef]
40. Smith, B.; Anovitz, L.M. IV.F.1 Lifecycle Verification of Polymeric Storage Liners. Available online: [https://www.hydrogen.energy.gov/pdfs/progress13/iv\\_f\\_1\\_smith\\_2013.pdf](https://www.hydrogen.energy.gov/pdfs/progress13/iv_f_1_smith_2013.pdf) (accessed on 14 July 2021).
41. Flaconnèche, B.; Martin, J.; Klopffer, M.H. Permeability, Diffusion and Solubility of Gases in Polyethylene, Polyamide 11 and Poly (Vinylidene Fluoride). *Oil Gas Sci. Technol.* **2006**, *56*, 261–278. [CrossRef]
42. Klopffer, M.H.; Berne, P.; Weber, M.; Castagnet, S.; Hochstetter, G.; Espuche, E. New materials for hydrogen distribution networks: Materials development & technico-economic benchmark. *Diffus. Mater. Dimat* **2011**, *2012*, 323, 407–412. [CrossRef]
43. Kunz, D.A.; Schmid, J.; Feicht, P.; Erath, J.; Fery, A.; Breu, J. Clay-Based Nanocomposite Coating for Flexible Optoelectronics Applying Commercial Polymers. *ACS Nano* **2013**, *7*, 4275–4280. [CrossRef] [PubMed]
44. DeRocher, J.P.; Gettelfinger, B.T.; Wang, J.S.; Nuxoll, E.E.; Cussler, E.L. Barrier membranes with different sizes of aligned flakes. *J. Membr. Sci.* **2005**, *254*, 21–30. [CrossRef]
45. Sun, Y.; Lv, H.; Zhou, W.; Zhang, C. Research on hydrogen permeability of polyamide 6 as the liner material for type IV hydrogen storage tank. *Int. J. Hydrog. Energy* **2020**, *45*, 24980–24990. [CrossRef]
46. Ebina, T.; Ishii, R.; Aizawa, T.; Yoshida, H. Development of Clay-based Film and Its Application to Gas Barrier Layers of Composite Tanks. *J. Jpn. Pet. Inst.* **2017**, *60*, 121–126. [CrossRef]
47. Picard, E.; Gérard, J.F.; Espuche, E. Reinforcement of the Gas Barrier Properties of Polyethylene and Polyamide Through the Nanocomposite Approach: Key Factors and Limitations. *Oil Gas Sci. Technol. Rev. d'IFP Energ. Nouv.* **2013**, *70*, 237–249. [CrossRef]
48. Ismail, A.F.; Lorna, W. Penetrant-induced plasticization phenomenon in glassy polymers for gas separation membrane. *Sep. Purif. Technol.* **2002**, *27*, 173–194. [CrossRef]
49. Minelli, M.; Oradei, S.; Fiorini, M.; Sarti, G.C. CO<sub>2</sub> plasticization effect on glassy polymeric membranes. *Polymer* **2019**, *163*, 29–35. [CrossRef]
50. Barrer, R.; Barrie, J.; Slater, J. Sorption and diffusion in ethyl cellulose. Part III. Comparison between ethyl cellulose and rubber. *J. Polym. Sci.* **1958**, *27*, 177–197. [CrossRef]
51. Fleming, G.K.; Koros, W.J. Dilation of polymers by sorption of carbon dioxide at elevated pressures. 1. Silicone rubber and unconditioned polycarbonate. *Macromolecules* **1986**, *19*, 2285–2291. [CrossRef]
52. Jordan, S.S.; Koros, W.J. A free volume distribution model of gas sorption and dilation in glassy polymers. *Macromolecules* **1995**, *28*, 2228–2235. [CrossRef]
53. Koros, W.J.; Paul, D.R.; Rocha, A.A. Carbon dioxide sorption and transport in polycarbonate. *J. Polym. Sci. Polym. Phys. Ed.* **1976**, *14*, 687–702. [CrossRef]
54. Paul, D.R.; Koros, W.J. Effect of partially immobilizing sorption on permeability and the diffusion time lag. *J. Polym. Sci. Polym. Phys. Ed.* **1976**, *14*, 675–685. [CrossRef]
55. Aminabhavi, T.M.; Aithal, U.S.; Shukla, S.S. An overview of the theoretical models used to predict transport of small molecules through polymer membranes. *Polym. Rev.* **1988**, *28*, 421–474. [CrossRef]
56. Bondar, V.I.; Kamiya, Y.; Yampol'Skii, Y.P. On pressure dependence of the parameters of the dual-mode sorption model. *J. Polym. Sci. Part B Polym. Phys.* **1996**, *34*, 369–378. [CrossRef]
57. Pace, R.; Datsyner, A. Statistical mechanical model of diffusion of complex penetrants in polymers. II. Applications. *J. Polym. Sci. Polym. Phys. Ed.* **1979**, *17*, 1693–1708. [CrossRef]
58. Raucher, D.; Sefcik, M.D. Gas transport and cooperative main-chain motions in glassy polymers. *Ind. Gas Sep.* **1983**, 89–110.
59. Raucher, D.; Sefcik, M.D. *Sorption and Transport in Glassy Polymers: Gas—Polymer—Matrix Model*; American Chemical Society: Washington, DC, USA, 1983.
60. Minelli, M.; Campagnoli, S.; De Angelis, M.G.; Doghieri, F.; Sarti, G.C. Predictive Model for the Solubility of Fluid Mixtures in Glassy Polymers. *Macromolecules* **2011**, *44*, 4852–4862. [CrossRef]
61. Galizia, M.; De Angelis, M.G.; Sarti, G.C. Sorption of hydrocarbons and alcohols in addition-type poly (trimethyl silyl norbornene) and other high free volume glassy polymers. II: NELF model predictions. *J. Membr. Sci.* **2012**, *405*, 201–211. [CrossRef]
62. Minelli, M.; Sarti, G.C. Permeability and diffusivity of CO<sub>2</sub> in glassy polymers with and without plasticization. *J. Membr. Sci.* **2013**, *435*, 176–185. [CrossRef]
63. Sanchez, I.C.; Lacombe, R.H. Statistical Thermodynamics of Polymer-Solutions. *Macromolecules* **1978**, *11*, 1145–1156. [CrossRef]
64. Minelli, M.; Sarti, G.C. Gas permeability in glassy polymers: A thermodynamic approach. *Fluid Phase Equilibria* **2016**, *424*, 44–51. [CrossRef]

65. Minelli, M.; Sarti, G.C. Thermodynamic model for the permeability of light gases in glassy polymers. *AIChE J.* **2015**, *61*, 2776–2788. [[CrossRef](#)]
66. Rodgers, P.A. Pressure Volume Temperature Relationships for Polymeric Liquids—A Review of Equations of State and Their Characteristic Parameters for 56 Polymers. *J. Appl. Polym. Sci.* **1993**, *48*, 1061–1080. [[CrossRef](#)]
67. Minelli, M.; Sarti, G.C. Elementary prediction of gas permeability in glassy polymers. *J. Membr. Sci.* **2017**, *521*, 73–83. [[CrossRef](#)]
68. Bondi, A.V. van der Waals volumes and radii. *J. Phys. Chem.* **1964**, *68*, 441–451. [[CrossRef](#)]
69. Fujita, H.; Kishimoto, A.; Matsumoto, K. Concentration and temperature dependence of diffusion coefficients for systems polymethyl acrylate and n-alkyl acetates. *Trans. Faraday Soc.* **1960**, *56*, 424–437. [[CrossRef](#)]
70. Doolittle, A.K. Studies in Newtonian flow. II. The dependence of the viscosity of liquids on free-space. *J. Appl. Phys.* **1951**, *22*, 1471–1475. [[CrossRef](#)]
71. Doolittle, A.K. Studies in Newtonian flow. III. The dependence of the viscosity of liquids on molecular weight and free space (in homologous series). *J. Appl. Phys.* **1952**, *23*, 236–239. [[CrossRef](#)]
72. Peterlin, A. Dependence of diffusive transport on morphology of crystalline polymers. *J. Macromol. Sci. Part B Phys.* **1975**, *11*, 57–87. [[CrossRef](#)]